ЯДЕРНА ФІЗИКА ТА ЕНЕРГЕТИКА / NUCL. PHYS. AT. ENERGY 27 (2026) 248–258 ISSN 1818-331X

РАДІАЦІЙНА ФІЗИКА
RADIATION PHYSICS

УДК 539.184.2 https://doi.org/10.15407/jnpae2026.03.248

**V. K. Garg[1], M. Gupta[1], M. K. Tiwari[2], A. Sharma[1,]***

[1] *Chitkara School of Engineering and Technology, Chitkara University, Himachal Pradesh, India*
[2] *Raja Ramanna Centre for Advanced Technology, Indore, India*

*Corresponding author: ajay.sharma@chitkarauniversity.edu.in

# THEORETICAL INSIGHTS INTO *L* X-RAY EMISSION ANISOTROPY AND POLARIZATION IN HIGH-*Z* ELEMENTS

A comprehensive theoretical study of the angular anisotropy and linear polarization of characteristic *L*-shell X-ray emission from high-*Z* atoms (tantalum, tungsten, rhenium, iridium, gold, and thallium) produced by photoionization with unpolarized photons is reported. The calculations are performed within the non-dipole approximation employing three alternative descriptions of the atomic potential: (i) point Coulomb field, (ii) screened Coulomb field, and (iii) analytical perturbative treatment. To examine only direct *L*-shell fluorescence, the incident photon energy is limited to the range extending from the $L_3$ absorption threshold to the *K*-shell edge, thereby eliminating contributions from *K*-shell ionization, Coster–Kronig transitions, and inter-shell vacancy transfer processes. The degree of linear polarization for the $L_\ell$, $L_{\alpha 1}$, and $L_{\alpha 2}$ spectral lines is calculated up to 60 keV to determine their variation with excitation energy. The results indicate that vacancy alignment reaches its maximum close to the threshold, where great changes in subshell ionization amplitudes and photoelectron partial-wave components occur. As the photon energy increases, the alignment progressively decreases, leading to reduced anisotropy and polarization, and gradually approaches a slowly varying high-energy limit. The $L_\ell$ transition consistently shows greater anisotropy than the $L_\alpha$ lines, while the polarization values of $L_\ell$, $L_{\alpha 1}$, and $L_{\alpha 2}$ remain transition-specific because of differences in angular momentum coupling and radiative transition matrix elements. A systematic dependence on atomic number is observed throughout the investigated elements, with heavier atoms exhibiting comparatively greater changes in the polarization behaviour. While this trend may reflect the combined influence of relativistic effects, spin-orbit coupling, and electron-correlation effects commonly associated with heavier atomic systems. Although all three theoretical approaches predict similar overall energy-dependent trends, noticeable quantitative differences are obtained in the polarization magnitudes, demonstrating the sensitivity of the results to the adopted potential model and alignment treatment. Comparison with previously published results of Kämpfer et al. and Özdemir et al. confirms the consistency of the present calculations and $L_\alpha$ offers a deeper theoretical understanding of the combined influence of vacancy alignment, multipole mixing, and relativistic dynamics in *L*-shell X-ray emission.

*Keywords: L*-shell X-ray emission, polarization, anisotropy, photoionization, high-*Z* atoms.

## 1. Introduction

The study of angular anisotropy and linear polarization in characteristic X-ray emissions is essential for the understanding of the basic processes of photoionization at the atomic level, especially in the case of the high-*Z* elements in which the relativistic and non-dipole effects come into play. Moreover, these parameters are used to study the exchange of coupling between subshells, transition probabilities and fine structure analysis of multipole transitions. Since the *K*-shell has been investigated extensively, the *L*-shell ionization shows unique behaviour of electron-photon interaction, particularly under conditions in which radiation emission is significantly affected by multipole interferences and correlation effects.

According to [1], non-dipole contributions to electron-photon interactions can influence the linear polarization of characteristic radiation from neon-like $Fe^{16+}$ and $U^{82+}$ ions in $L_3$ photoionization processes. Meanwhile, the polarization of L X-rays for some elements at 59.54 keV energy has been calculated by Özdemir et al. [2], and it was noticed that the linear polarization of $L_\ell$ lines is greater than that of $L_\alpha$ lines.

Moreover, the alignment of inner-shell vacancies produced in heavy elements following photoionization or electron-impact ionization can be investigated through measurements of the angular distribution and linear polarization of the emitted characteristic X-rays as analyzed by Jitschin and Werner [3]. These quantities are commonly described using alignment parameters, which depend on the atomic structure, the energy of the incident radiation, and the polarization state of the exciting photons. Theoretical and experimental studies by Wu et al. [4] and Han and Demir [5] examined the anisotropy and polarization characteristics of *L*-shell X-rays in heavy elements. Their investigations showed that, for photon-induced *L* X-ray emission in gold and lead atoms, the anisotropy and linear polarization above the $L_3$ absorption edge are relatively small. Furthermore, anisotropy aids in describing the alignment parameter $A_2$ and, henceforth, the linear polarization of heavy elements (high--$Z$). However, the angular distribution measurements are challenging and require corrections for both the absorbed beam and produced photons, which in turn may lead to errors.

Several studies have explained the linear polarization in terms of the alignment parameter, calculated by means of several approximation methods. Kämpfer et al. [6] calculated linear polarization for tungsten with the help of density matrix theory; the results are in agreement with experimental results and exposed a weak susceptibility of polarization on incident radiation.

Singh et al. [7] examined alignment in lead, thorium, and uranium elements by intensity measurements in the case of the $L_3$ sub-shell using selective photoionization by an unpolarized radiation of 59.54 keV. The precise measurements undeniably concluded that anisotropy, if any, in the $L_3$ X-ray is very small and is nearly of the order of the theoretically measured value.

In 2018, Sharma et al. [8] reported that the experimentally observed anisotropy values were higher than those predicted theoretically. Further, $L_\ell$ lines are observed to be more anisotropic than uncertain $L_{\alpha1}$ and $L_{\alpha2}$ lines with opposite anisotropies. Additionally, Sharma et al. [8] have shown that formulations and interpretations given for the study of photon-induced inner shell alignment of atoms are valid and concluded that the experimental trends in the alignment parameter are consistent with each other. Similar alignment trends are observed in ytterbium also. The maximum number of alignment studies is performed for $L$ sub-shell electrons excited by 26 and 60 keV, or near threshold energies for the sub-shells.

Variation in the alignment parameter leads to a distinction in polarization for all the high-$Z$ elements. It is observed that the approximation method, atomic state and incident photon energy affect anisotropy and thus the polarization. Zhang et al. [9] recognized that the linear polarization of the characteristic photons is significantly improved because of the transference of polarization from the linearly polarized incident ionizing photons. Garg et al. [10] measured the anisotropy by changing the incident radiation energy from $L_3$ edge to 60 keV (where the majority of experimental results are available) in the angular range of 0 to 180°. Multiple ionization of vacancies occurs in the case of ionization by high ions and not in the case of ionization by photons; that is, alignment studies initiated by photoionization have an immaterial multiple ionization effect. Hence, it is viable to ionize a specific atomic sub-shell by monitoring photon ionising beam energy and to avoid conflict due to the Coster–Kronig transition with the alignment measurement studies by means of selective excitations.

The anisotropy in $L_\ell$ line is more compared to $L_\alpha$ lines, which is a combination of unresolved $L_{\alpha1}$ and $L_{\alpha2}$ lines with converse anisotropy [11]. Wu et al. [12] used the relativistic single-configuration Dirac–Hartree–Fock method to study anisotropy for barium, ytterbium, mercury, and radon atoms with closed subshells and observed that the $L_{\alpha1}$ lines are nearly isotropic and $L_{\alpha2}$, $L_\ell$ lines are feebly anisotropic. Luo et al. [13] investigated the dependence of L-RR X-ray polarization on energy and atomic number $Z$ and found that the results are in good agreement with $K$-shell experimental values and are nearer to $L$-shells. As vacancy alignment is sensitive to the model or approximation method used, this will also affect the degree of linear polarization of the atoms under investigation [14].

Käbisch et al. [15] and Alqadi et al. [16] used synchrotron radiation to investigate $L$-shell fluorescence of various elements; furthermore, Alqadi et al. compared results in good agreement with the Dirac–Hartree–Slater model and prior datasets. The photoelectron-based angular distribution of krypton was measured with the help of linearly polarized synchrotron radiation in the neighbourhood of the resonant excitations of the $L_3$ subshell and huge non-dipole involvement has been detected [17]. The impact energy dependency of $L$-shell X-ray production cross sections of lead ($Z = 82$) has been measured in the range of 15–30 keV electrons. The observations were carried out using the thick target method, and the X-ray yields as well as the production cross sections of various $L$-subshell lines were measured and compared with the results of Monte Carlo simulations [18].

In the present study, an effort has been made to examine with high accuracy the linear polarization of the fluorescent radiation by means of a theoretically assessed alignment parameter. The studies are focused on polarization and alignment at incident photon energies near threshold to 60 keV to draw a distinction with the existing outcomes of Kämpfer et al. [6]. The incident photon energies have been selected to evade the $K$-shell binding energies to avoid the Coster–Kronig transitions and inner shell transfer to confirm the spectral purity.

## 2. Formulation

The present work investigates the angular distribution of characteristic $L$ X-ray lines inside the polarization plane, changing the azimuthal angle $\phi$ from 0 to 180° but keeping the polar angle $\theta$ at 90°. The $Z$ axis is the axis of the incoming photon beam, while the outgoing radiation lies in the XY plane (Fig. 1). Such a geometry is appropriate for the investigation of linear polarization effects as well as anisotropic emission in photo-ionized atoms.

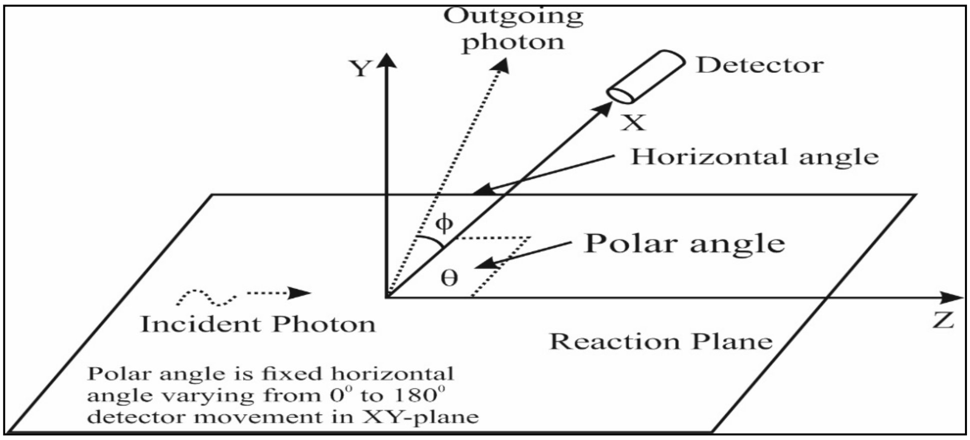


Fig. 1. Coordinate system to study angular distribution and linear polarization.

In this configuration, the azimuthal angle $\phi$ is defined as the angle between the projection of the emitted photon onto the plane perpendicular to its propagation direction and the X-axis, which is aligned with the electric vector of the incident linearly polarized radiation. The polar angle $\theta$ denotes the angle between the incident photon beam and the emission direction. Within this reference frame, quantum-mechanical calculations enable a rigorous description of the angular distribution and degree of polarization of inner-shell X-ray transitions as a function of incident photon energy, with particular relevance to *L*- and *K*-shell processes [6].

Fig. 1 shows the coordinate system to which the geometry of the problem is referred to study the linear polarization properties of the characteristic X-ray fluorescence as a function of the incident photon energy. The incident radiation propagates along the Z-axis, while the emitted radiation lies in the XY-plane, perpendicular to the direction of the photon beam. Here, $\phi$ denotes the azimuthal angle, defined as the angle between the projected X-ray emission vector and the X-axis (i.e., the direction of the electric field vector of the incident linearly polarized photon). Following Kämpfer et al. [6], the polar angle $\theta$ is defined as the angle between the direction of the incident photon (Z-axis) and that of the emitted photon. The geometry adopted in the present work is well suited for investigating the angular anisotropy and linear polarization of *L*-shell characteristic X-rays following photoionization. In this configuration, the emitted radiation is observed perpendicular to the incident photon beam, while the azimuthal angle is measured relative to the electric-field vector of the incident polarized radiation. Such an arrangement enhances the sensitivity to vacancy alignment effects and facilitates a clearer analysis of the anisotropic and polarization behaviour of the emitted X-rays. This geometry is highly advantageous for the analysis of *L*-shell X-rays, including their anisotropy and polarization associated with inner-shell photoionization under linear polarization conditions. In the case of grazing incidence for fully linearly polarized X-rays along the X-direction $\phi = 0°$, the angular distribution for each $L_g$ peak follows the formulation given in [8].

$$WL_g\left(90°, 0°\right) = \omega\,, \tag{1}$$

where $\omega = \dfrac{W_0}{4\pi}\left(1+\alpha_2\left[\left(-1.25\right)\mathrm{A}_{20}\right]\right)$.

On the similar lines for $\phi$ = 30, 60, 90, 120, 150 and 180°:

$$WL_g\left(90°, 30°\right) = \omega + c_1\alpha_2\,, \tag{2}$$

$$WL_g\left(90°, 60°\right) = \omega + 3c_1\alpha_2\,, \tag{3}$$

$$WL_g\left(90°, 90°\right) = \omega + 4c_1\alpha_2\,, \tag{4}$$

$$WL_g\left(90°, 120°\right) = \omega + 3c_1\alpha_2\,, \tag{5}$$

$$WL_g\left(90°, 150°\right) = \omega + c_1\alpha_2\,, \tag{6}$$

$$WL_g\left(90°, 180°\right) = \omega\,, \tag{7}$$

where $c_1 = \dfrac{W_0}{4\pi}\left[\left(0.375\right)\mathrm{A}_{20}\right]$.

At every angle $\phi$, for each $L_g$ peak, $W_0/4\pi$ is constat and only $\alpha_2$ that determined by *J* values of the initial and final states of the ion, having values 0.5, 0.1, –0.4 and 0.1 for $L_\ell$, $L_{\alpha1}$, $L_{\alpha2}$ and $L_{\beta2}$ lines correspondingly [16].

The normalized intensities for each $L_g$ peak of *L* X-rays at an azimuthal angle (e. g. $\phi = 0°$) is expressed as

$$\frac{WL_g(90°,0°)}{WL_g(90°,90°)} = \frac{\omega}{\omega + 4c_1\alpha_2}. \quad (8)$$

For individual $L_\ell$, and $L_\alpha$ peaks the normalized intensities at $\phi = 0°$ can be measured by using equations (9) and (10) respectively

$$\frac{WL_\ell(90°,0°)}{WL_\ell(90°,90°)} = \frac{\omega}{\omega + 4c_1\alpha_2}, \quad (9)$$

$$\frac{WL_\alpha(90°,0°)}{WL_\alpha(90°,90°)} =$$

$$= \frac{\omega + \frac{W_0}{4\pi}\left(1 + \alpha_2\left[A_{20}(-1.25)\right]\right)}{\omega + 4c_1\alpha_2 + \frac{W_0}{4\pi}\left(1 + \alpha_2\left[A_{20}(0.250)\right]\right)}. \quad (10)$$

Afterwards, the derived $A_{20}$ alignment parameter, calculated via non-relativistic dipole approximation (NDA), i) point Coulomb, ii) screened Coulomb, and iii) analytical perturbation theory, is used in Eqs. (9) and (10) to study the azimuthal behaviour of the $L_\alpha$ and $L_\ell$ X-ray lines at an angle $\phi$ between 0 and 180°. Given that $L_\alpha$ and $L_\ell$ transitions are generated by photoionization of the $L_3$ subshell, the maximum anisotropy in the angular emission is anticipated near the ionization threshold. Therefore, in this work, the alignment parameters have been evaluated at photon energies lying between the $L_3$ and $L_2$ binding energies of the target atoms, where strong anisotropy is present and at 60 keV, corresponding to a higher energy, where an abundance of experimental data is available. The angular distribution studies were performed at various azimuthal angles, in the interval of 30°, from 0 to 180°, the full range.

Furthermore, the degree of linear polarization of the emitted characteristic X-rays is of particular interest for studying the polarization properties of an X-ray source in detail, indicating the degree of anisotropy of the photon emission. Since the anisotropy in the angular distribution originates from a non-uniform population of the magnetic sublevels, the resulting linear polarization of the emitted radiation becomes a direct observable consequence of this anisotropy. Therefore, a larger magnitude produces stronger directional asymmetry in the emission pattern and consequently a larger value of the first Stokes parameter $P_1$, which serves as a quantitative indicator of the anisotropy of the emitted X-rays. This is summarized by the parameter $P_1$, which quantifies the linearly polarized component of the radiation. Concerning inner-shell photoionization processes produced by an unpolarized photon beam, $P_1$ is a direct measure of the anisotropy in the emission pattern, and it is intrinsically related to the alignment parameter $A_2$ of the initial vacancy state. In particular, for emissions along the normal to the incident beam direction, $\theta = 90°$, the linear polarization of lines $L_{\alpha1}$, $L_{\alpha2}$, and $L_\ell$ can be calculated using analytic equations that provide $P_1$ as a function of the previously obtained $A_{20}$. Based on the angular momentum coupling and quantum electrodynamical formalism used in [6] and Zhang et al. [9], these contributions provide the transformation of the atomic alignment into polarimetric observables, connecting the study of the angular distribution with the analysis of the polarization in a single theoretical approach.

## 3. Results and discussions

### 3.1. Angular distribution studies

The theoretical analysis of the angular distribution for characteristic *L* ($L_\alpha$ and $L_\ell$) X-ray emission lines was performed for some high-*Z* elements (tantalum, tungsten, rhenium, iridium, gold, and thallium) over a wide range of the incident energy from threshold up to 60 keV. At Low photon energies, the calculated normalized intensities as a function of the azimuthal angle ($\phi$) in the vicinity of the $L_3$ subshell threshold clearly indicate a distinct anisotropy for all the elements mentioned above.

As shown in Fig. 2, three models converge perfectly at 90°, where the normalized angular distribution reaches its maximum value of 1.00. This indicates that for transitions in tungsten ($_{74}$W) at this energy, the emission is most intense perpendicular to the reference axis. The gap between the screened and Coulomb lines illustrates the importance of electron-electron interactions. In heavy elements like tungsten, the inner electrons significantly shield the outer ones from the full positive charge of the nucleus, which shifts the probability of X-ray emission.

The most dramatic difference occurs between 0 and 60°. The analytical perturbation theory shows a much steeper drop-off as the angle approaches 0°. This suggests that the perturbation approximation may fail to capture the full complexity of the atomic field near the forward-scattering direction compared to potential-based models.

The distribution is anisotropic, meaning it is not the same in all directions. If the emission were isotropic (equal in all directions), the graph would be a flat horizontal line. The curvature proves that the physical process of emission has a preferred spatial orientation.

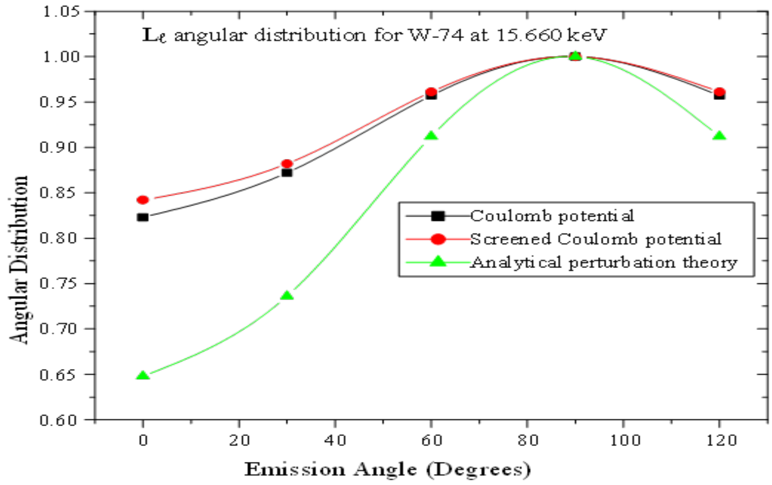


Fig. 2. Normalized $L_\ell$ angular distribution of $_{74}$W at incident photon energy 15.660 keV using NDA: *black curve* – point Coulomb, *red curve* – screened Coulomb, and *green curve* – analytical perturbation theory. (See color Figure on the journal website.)

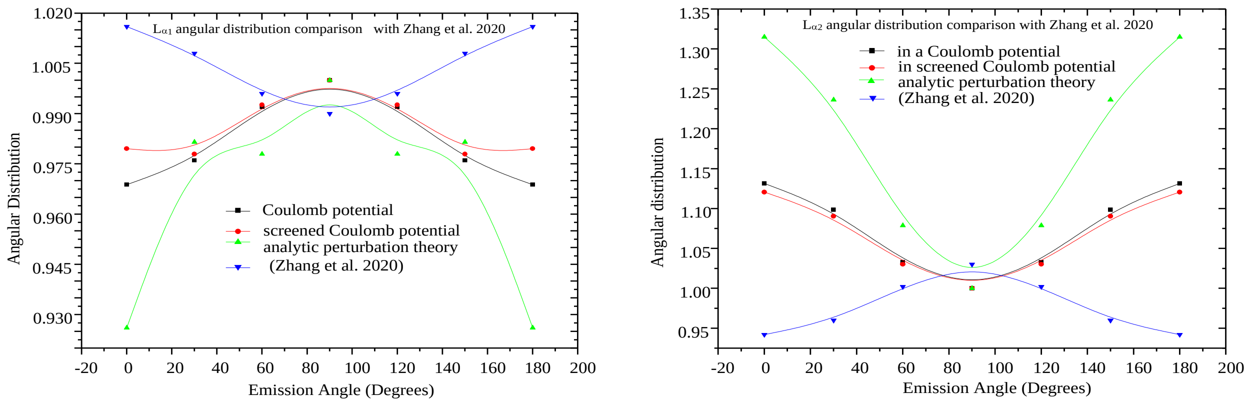


Fig. 3. Comparison of present angular distribution results for $L_\ell$, $L_{\alpha1}$, and $L_{\alpha2}$ of $_{74}$W at 15.660 keV with that of Zhang et al. [9]. (See color Figure on the journal website.)

As it is clear from the graphs (Figs. 2 and 3), the present results demonstrate a comparable variation of all $L_\ell$ and $L_\alpha$ relative intensities for incident photon energy 15.660 keV. The intensities rise with the rise in angle from 0 to 90°, and after 90° there is a drop. Furthermore, it is found that the $L_\ell$ X-ray groups exhibit greater variability than the $L_\alpha$ X-ray groups. The reason for the more significant variance of $L_\ell$ X-rays compared to $L_\alpha$ could be that the $L_\ell$ group only has one intense line ($L_3 - M_1$), while the $L_\alpha$ group has two lines, $L_{\alpha1}$ ($L_3 - M_5$) and $L_{\alpha2}$ ($L_3 - M_4$), which have opposite anisotropic distributions.

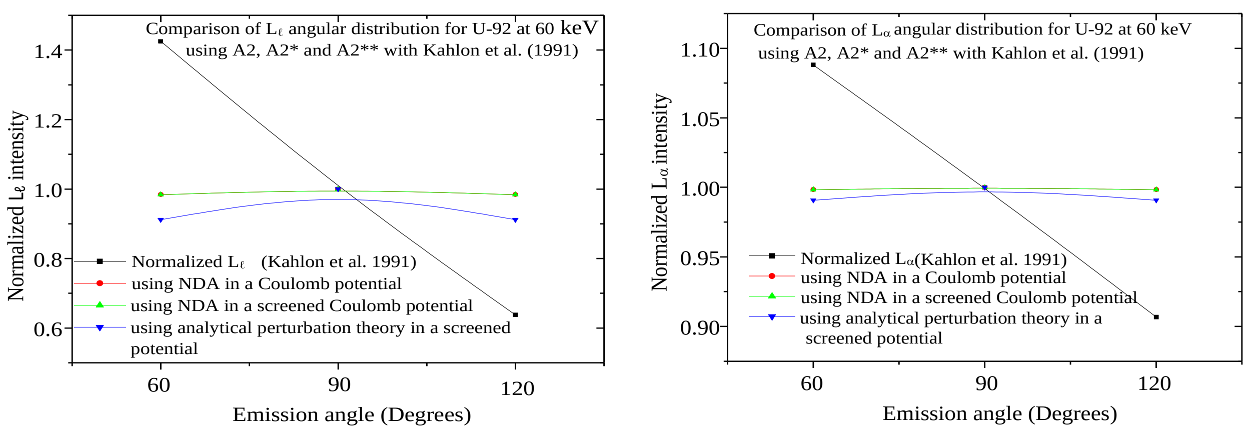


Fig. 4. Comparison of present angular distribution results for $L_\ell$ and $L_\alpha$ of $^{92}$U at 60 keV with Kahlon et al. [19]. (See color Figure on the journal website.)

As observed in Fig. 4 when compared with Kahlon et al. [19], the anisotropy for *W* at 60 keV is very small for both $L_\ell$ and $L_\alpha$ lines. However, the magnitude of anisotropy at 60 keV is considerably reduced compared to that near threshold energies, reflecting the diminishing influence of alignment effects at higher excitation energies except in the case of analytical perturbation theory, where this reduction is minimal, as illustrated in Figs. 3 and 4. Comparison with the angular distribution data of tungsten ($_{74}$W) at 15.660 keV reported by Zhang et al. [9] further validates the present results.

Quantitatively, the anisotropy values predicted by analytical perturbation theory are significantly higher than those obtained using the other two approaches, namely the non-relativistic distorted-wave approximation with (i) a point Coulomb potential and (ii) a screened Coulomb potential, particularly at both photon energies. This discrepancy may be attributed to the treatment of screening effects and the inclusion of isotropic correction factors within the analytical perturbation framework, which likely enhance the predicted anisotropy relative to the other models. Furthermore, the angular distribution profiles derived using the analytically obtained alignment parameters are found to be relatively uniform across both elements and exhibit similar behaviour at both photon energies, suggesting a degree of robustness and energy independence in this approximation [14].

## 4. Polarization studies

In the present investigation, the degree of linear polarization of characteristic *L*-shell X-ray lines has been evaluated through the alignment parameter $A_{20}$, which quantifies the spatial anisotropy of the initial vacancy state following photoionization. Since alignment is inherently sensitive to the incident photon energy as well as to the theoretical model employed for its computation, its variation provides a direct framework for interpreting the behaviour of linear polarization (Table). Fig. 5 illustrates the dependence of $A_{20}$ on photon energy for tantalum, serving as a representative case.

**Degree of linear polarization of *L* X-rays for $_{73}$Ta in the energy range of 13 to 60 keV incident photon energy**

| Sr. No. | Incident photon energy, keV | P($L_{\alpha1}$) Using the alignment parameter ($A_{20}$, $A_{20}^*$, $A_{20}^{**}$) | | | P($L_{\alpha2}$) Using the alignment parameter ($A_{20}$, $A_{20}^*$, $A_{20}^{**}$) | | | Incident photon energy, keV | Polarization values of Kämpfer et al. [6] | |
|---|---|---|---|---|---|---|---|---|---|---|
| | | $A_{20}$ | $A_{20}^*$ | $A_{20}^{**}$ | $A_{20}$ | $A_{20}^*$ | $A_{20}^{**}$ | | P($L_{\alpha1}$) | P($L_{\alpha2}$) |
| 1 | 13 | 0.0466 | 0.0433 | 0.0767 | –0.1730 | –0.2301 | –0.2722 | 10.307 | 1.02 | –5.2 |
| 2 | 15 | 0.0333 | 0.0306 | 0.0767 | –0.1264 | –0.1595 | –0.2722 | 12 | 1.04 | –5.6 |
| 3 | 20 | 0.0205 | 0.0191 | 0.0767 | –0.0794 | –0.0983 | –0.2722 | 14 | 1.06 | –5.8 |
| 4 | 25 | 0.0162 | 0.0153 | 0.0767 | –0.0634 | –0.0785 | –0.2722 | 16 | 1.08 | –6.2 |
| 5 | 30 | 0.0143 | 0.0137 | 0.0767 | –0.0559 | –0.0699 | –0.2722 | 18 | 1.10 | –6.4 |
| 6 | 35 | 0.0132 | 0.0127 | 0.0767 | –0.0518 | –0.0650 | –0.2722 | 20 | 1.12 | –6.6 |
| 7 | 40 | 0.0125 | 0.0121 | 0.0767 | –0.0489 | –0.0619 | –0.2722 | 22 | 1.15 | –6.8 |
| 8 | 45 | 0.0120 | 0.0117 | 0.0767 | –0.0472 | –0.0597 | –0.2722 | NA | NA | NA |
| 9 | 50 | 0.0117 | 0.0203 | 0.0767 | –0.0460 | –0.1047 | –0.2722 | NA | NA | NA |
| 10 | 55 | 0.0114 | 0.0112 | 0.0767 | –0.0449 | –0.0573 | –0.2722 | NA | NA | NA |
| 11 | 60 | 0.0112 | 0.0110 | 0.0767 | –0.0443 | –0.0559 | –0.2722 | NA | NA | NA |

*Note*. The polarization values reported from Kämpfer et al. [6] are expressed in percentage, %.

At very high photon energies, the incident photon effectively interacts with the electron as if it were quasi-free. Consequently, the detailed structure of the atomic potential (i.e., the specific “shape” of the atom) becomes less significant compared to the large kinetic energy involved in the interaction, leading to a reduction in alignment. The largest discrepancies are observed near the ionization threshold (10–20 keV). The point Coulomb potential predicts a pronounced negative alignment, whereas the screened Coulomb potential yields a comparatively weak positive alignment. This strong sensitivity in the near-threshold region indicates that electron screening effects play a crucial role in determining the post-photoionization spatial alignment of tantalum ($Z = 73$) ions. The marked discrepancy between the two models highlights the necessity of incorporating many-electron interactions in the theoretical description of heavy atomic systems, as the use of a pure Coulomb potential leads to substantially different (and negative) alignment predictions.

With increasing photon energy ($E \gtrsim 50$ keV), the alignment effects are significantly reduced. In this high-energy regime, the interaction increasingly resembles that of a quasi-free electron, thereby diminishing the influence of the atomic potential.

Consequently, the dependence on the choice of potential model becomes weak, and the alignment parameter approaches an approximately energy-independent, near-zero value.

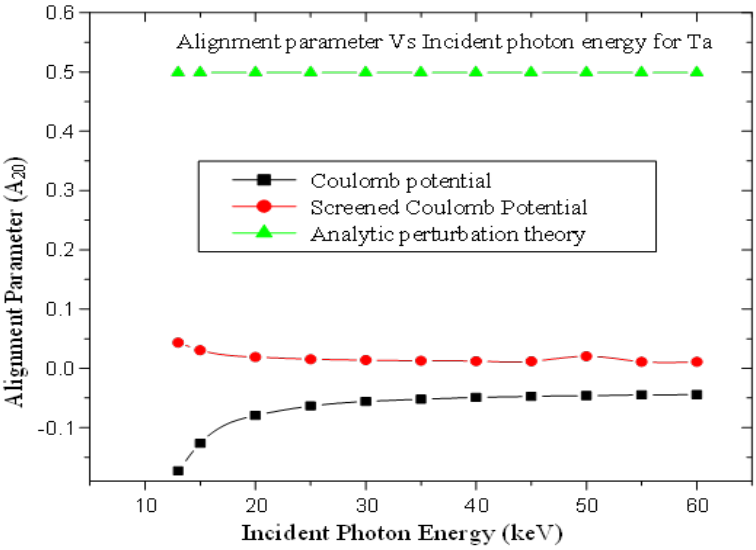


Fig. 5. Alignment parameter vs. incident photon energy for $_{73}$Ta. (See color Figure on the journal website.)

The linear polarization of $L_{\alpha1}$ and $L_{\alpha2}$ X-rays have been investigated as a function of incident photon energy in the range 13–60 keV (see Table) using different alignment parameters ($A_{20}$, $A_{20}^{*}$, $A_{20}^{**}$). The notation P($L_{\alpha1}$), P($L_{\alpha2}$), and P($L_{\ell}$) denotes the degree of linear polarization associated with the correspon-ding characteristic *L*-shell X-ray transitions. The results show a clear energy dependence of polarization, where P($L_{\alpha1}$) remains positive and decreases steadily with increasing photon energy, indicating a gradual reduction in the degree of linear polarization parallel to the reference plane. In contrast, P($L_{\alpha2}$) is negative throughout the energy range, with its magnitude varying with an increase in incident photon energy, signifying polarization perpendicular to that of $L_{\alpha1}$. This opposite behavior is consistent with the differing angular momentum coupling and selection rules governing the two transitions. The decreasing magnitude of polarization for both lines suggests a reduction in atomic alignment and a transition toward more isotropic emission at higher energies. The alignment parameters $A_{20}$ and $A_{20}^{*}$ yield consistent and physically meaningful trends, whereas $A_{20}^{**}$, being constant, fails to capture the energy dependence and represents a limiting approximation. A comparison with the results of Kämpfer et al. [6] shows qualitative agreement in the sign and trend of polarization but reveals significant quantitative differences in magnitude, likely due to differences in normalization or theoretical treatment. An anomalous deviation observed at 50 keV appears to be non-physical and may be attributed to numerical or typographical error. Overall, the analysis confirms that linear polarization of *L*-shell X-rays is strongly governed by atomic alignment effects and decreases with increasing incident photon energy.

Extending the present analysis, the degree of linear polarization was evaluated for four additional high-*Z* elements, namely tantalum, rhenium, iridium, gold, and thallium, over a broad range of incident photon energies from the ionization threshold up to 60 keV. The results indicate that, for all photon energies and across all investigated elements, the degree of linear polarization of the $L_{\ell}$ line consistently exceeds that of the $L_{\alpha1}$ and $L_{\alpha2}$ lines under all theoretical approximations considered. Furthermore, the polarization associated with the $L_{\alpha2}$ line exhibits a sign opposite to that of the $L_{\alpha1}$ line, in strong agreement with the results reported by Kämpfer et al. [6]. This inversion in polarization can be attributed to the differing angular momentum coupling characteristics of the corresponding radiative transitions. Specifically, the $L_{\alpha1}$ transition $3d_{5/2} \rightarrow 2p_{3/2}$ involves a change in the total angular momentum quantum number, whereas the $L_{\alpha2}$ transition $3d_{3/2} \rightarrow 2p_{3/2}$ does not, as also discussed by Kahlon et al. [19].

A clear distinction is observed in the predicted degree of polarization depending on the theoretical approach: analytical perturbation theory consistently yields higher polarization values compared to those obtained using NDA in point Coulomb or screened potentials. These results, compared using all three theoretical approximations $A_{20}$, $A_{20}^{*}$, and $A_{20}^{**}$ are presented in Figs. 6–9.

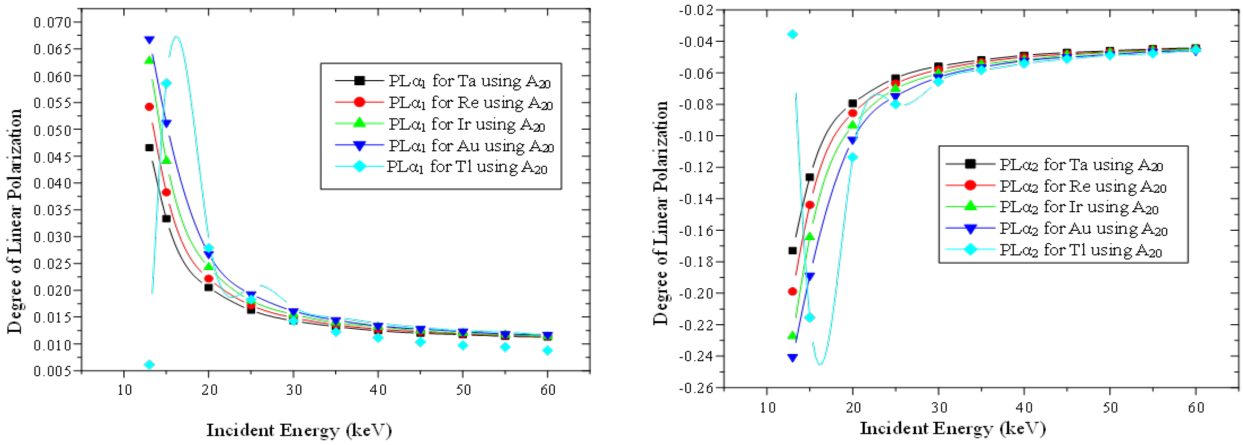


Fig. 6. P($L_{\alpha1}$) and P($L_{\alpha2}$) vs. incident photon energy for tantalum, rhenium, iridium, gold, and thallium using $A_{20}$. (See color Figure on the journal website.)

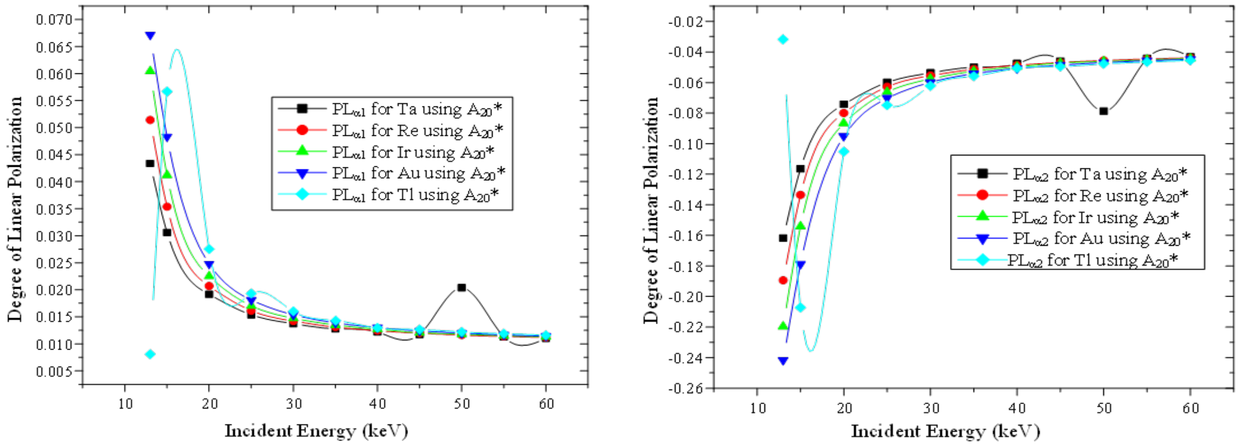


Fig. 7. P($L_{\alpha1}$) and P($L_{\alpha2}$) vs. incident photon energy for tantalum, rhenium, iridium, gold, and thallium using $A_{20}$*. (See color Figure on the journal website.)

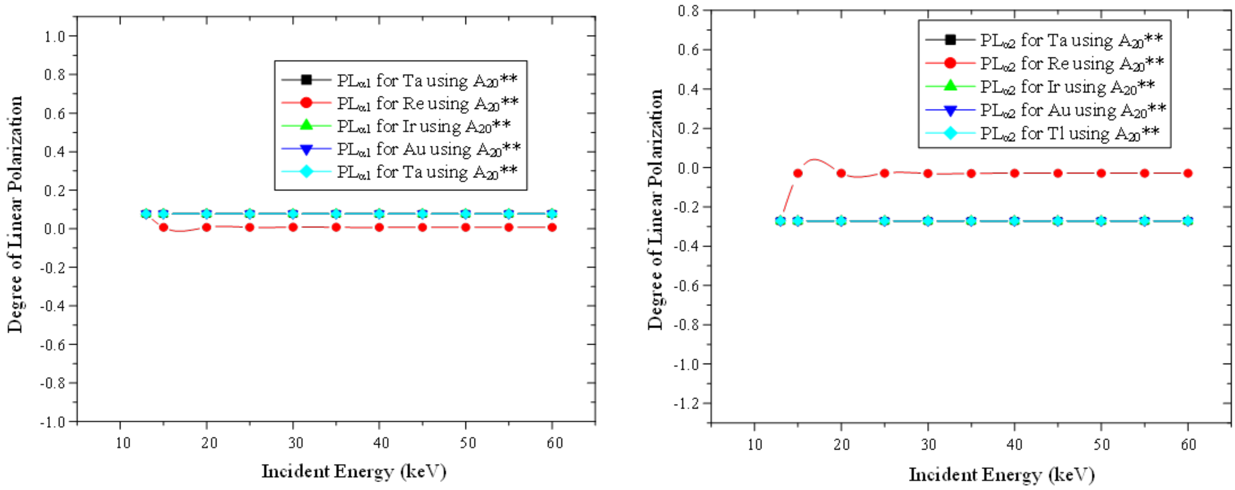


Fig. 8. P($L_{\alpha1}$) and P($L_{\alpha2}$) vs. incident photon energy for tantalum, rhenium, iridium, gold, and thallium using $A_{20}$**. (See color Figure on the journal website.)

Figs. 6–9 collectively demonstrate the dependence of the degree of linear polarization of the $L_{\alpha1}$, $L_{\alpha2}$, and $L_\ell$ characteristic X-ray lines on incident photon energy for tantalum, rhenium, iridium, gold, and thallium, evaluated using the three alignment parameter formulations $A_{20}$, $A_{20}^{*}$, and $A_{20}^{**}$. The degree of linear polarization of the $L_{\alpha1}$, $L_{\alpha2}$, and $L_\ell$ lines are directly dependent on the alignment parameters $A_{20}$, $A_{20}^{*}$, and $A_{20}^{**}$, which determine the anisotropic population of the initial *L*-shell vacancy states. Changes in these parameters modify the magnitude of polarization, while the general photon-energy dependence remains nearly unchanged. The differences in polarization among $L_{\alpha1}$, $L_{\alpha2}$, and $L_\ell$ arise from their distinct transition-specific angular momentum coupling coefficients.

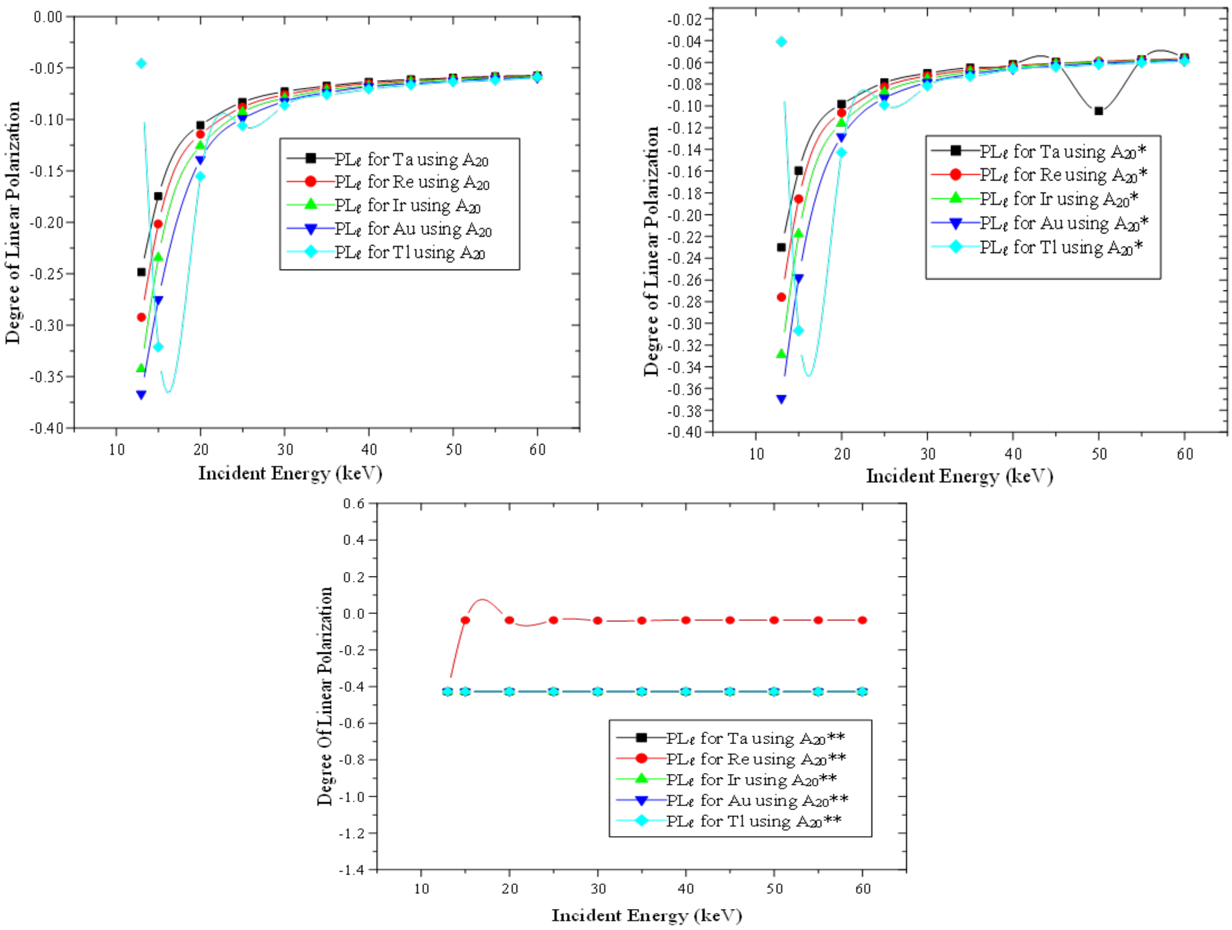


Fig. 9. P($L_\ell$) vs. incident photon energy for tantalum, rhenium, iridium, gold, and thallium using $A_{20}$, $A_{20}$*, and $A_{20}$**. (See color Figure on the journal website.)

The results consistently show that X-ray polarization is not constant, but varies systematically with excitation energy, confirming that the alignment of the initial $L$-shell vacancy state is strongly influenced by the photoionization dynamics. This energy sensitivity is most pronounced in the near-threshold region, where the photoelectron angular distribution and subshell ionization probabilities undergo rapid changes. The oscillatory manner observed for thallium in Figs. 6–8 is unlike represent a physical effect, since the alignment and polarization parameters are expected to vary with incident photon energy in heavy atoms. The asymmetrical variation for thallium ($Z = 81$) most likely originates from enhanced numerical sensitivity in the estimation of the alignment parameter, predominantly near the threshold region where relativistic effects, strong spin-orbit interaction, and subshell coupling become gradually significant. Because the polarization expression depends directly on alignment parameter, even small numerical deviations in the calculated alignment parameter may propagate and appear amplified in the polarization curves.

Across all figures, a common trend is the gradual evolution of polarization values with increasing photon energy after the threshold region, eventually approaching a more stable regime at higher energies. Such behaviour indicates that vacancy alignment becomes less sensitive to further increases in excitation energy once the dominant ionization channels are fully established. The smooth high-energy variation also suggests reduced influence of resonance-like effects and stronger averaging over competing excitation pathways.

The elemental sequence from tantalum to thallium reveals a clear atomic-number dependence of polarization behaviour. As $Z$ increases, the magnitude and slope of the polarization curves change noticeably, reflecting the growing importance of relativistic interactions, spin–orbit splitting, and electron correlation effects in heavy atoms. These factors alter both the population of magnetic sublevels in the ionized state and the angular momentum coupling during radiative decay. Consequently, heavier elements such as gold and thallium exhibit more distinct polarization responses compared with tantalum and rhenium. The comparison of $L_{\alpha1}$, $L_{\alpha2}$, and $L_\ell$ transitions further indicates that polarization is transition-specific. Since these lines originate from different final-state couplings and radiative selection pathways, their polarization magnitudes are not identical even under the same excitation conditions. This confirms that emitted X-ray polarization depends not only on the initial vacancy alignment but also on the multipole character and angular momentum properties of the particular transition. A comparison among $A_{20}$, $A_{20}^*$, and $A_{20}^{**}$ shows that while the overall energy-dependent trends remain similar, the absolute polarization values differ appreciably. This demonstrates that the theoretical treatment of vacancy alignment significantly affects quantitative predictions, although the underlying physical behaviour is preserved. The consistency of the general trends across all three models supports the robustness of the polarization mechanism, whereas the numerical differences emphasize the need for precise alignment parameter calculations in theoretical and experimental interpretation.

## 5. Conclusion

The present theoretical investigations establish that the angular distribution and linear polarization of *L*-shell characteristic X-ray lines ($L_{\alpha1}$, $L_{\alpha2}$, and $L_\ell$) emitted after photoionization of high-$Z$ atoms are direct manifestations of vacancy-state alignment produced during the primary ionization event. The calculated results for tantalum, rhenium, iridium, gold, and thallium show that the alignment parameters $A_{20}$, $A_{20}^*$, and $A_{20}^{**}$ govern the anisotropic population of magnetic sublevels and therefore determine both the magnitude of polarization and the angular anisotropy of the emitted radiation. A strong excitation-energy dependence is observed, particularly in the vicinity of the $L_3$ ionization threshold, where rapid changes in photoelectron partial-wave composition, subshell ionization cross sections, and channel interference generate mam alignment. As the incident photon energy increases, the alignment decreases monotonically, leading to a gradual reduction in polarization and anisotropy, and eventually approaches an asymptotic high-energy regime where the vacancy-state population becomes comparatively stable. This behaviour indicates that near-threshold dynamics dominate the polarization response, whereas high-energy excitation is controlled by more averaged continuum processes. For all elements and theoretical models considered, the $L_\ell$ transition exhibits consistently larger anisotropy than the $L_\alpha$ lines, indicating stronger alignment of the corresponding initial vacancy states. In contrast, the polarization magnitudes of $L_{\alpha1}$, $L_{\alpha2}$, and $L_\ell$ are not identical, owing to their distinct angular momentum coupling coefficients, multipole amplitudes, and radiative selection rules. Thus, the emitted X-ray polarization is governed jointly by the initial-state alignment and the transition-specific decay matrix elements. A systematic dependence on atomic number is also evident across the sequence tantalum–thallium. With increasing $Z$, the polarization curves exhibit modified slopes and magnitudes, reflecting the increasing influence of relativistic wavefunction contraction, spin-orbit splitting, and electron-correlation effects. These contributions alter both the magnetic-sublevel population created during ionization and the subsequent radiative decay dynamics, making polarization effects more pronounced in heavier atoms such as gold and thallium. Comparison among the three alignment formalisms demonstrates that, although all approaches reproduce the same qualitative energy dependence, significant quantitative deviations remain in the predicted polarization values, especially away from threshold and at higher photon energies. This sensitivity confirms that accurate treatment of vacancy alignment is essential for predictive modelling and that precision polarization measurements are required for stringent validation of competing theoretical descriptions. In summary, the study confirms that linear polarization and angular anisotropy of *L*-shell X-rays constitute sensitive probes of inner-shell photoionization dynamics, vacancy alignment, and relativistic atomic structure in heavy elements. The results provide an important theoretical basis for benchmarking photoionization calculations and for the development of polarization-resolved X-ray fluorescence techniques in synchrotron science, trace elemental analysis, and advanced spectroscopic diagnostics.

REFERENCES

1. A. Sharma, R. Mittal. Experimental and theoretical anisotropy studies for tungsten. Nucl. Instrum. Methods A 619 (2010) 55.
2. Y. Özdemir et al. L-shell polarization and alignment of heavy elements induced by 59.54 keV photons. Appl. Radiat. Isot. 69 (2011) 991.
3. W. Jitschin, U. Werner. X-ray and Auger-electron yields for quantitative element analysis. J. Vac. Sci. Technol. A 5 (1987) 1203.
4. Z.-W. Wu, J. Jiang, C.-Z. Dong. Influence of Breit interaction on the polarization of radiation following inner-shell electron-impact excitation of highly charged beryllium-like ions. Phys. Rev. A 84 (2011) 032713.
5. I. Han, L. Demir. Angular dependence of $L_3$-subshell X-ray emission following photoionisation. J. X-Ray Sci. Technol. 19 (2011) 13.
6. T. Kämpfer et al. Linear polarization of the charac-

teristic x-ray lines following inner-shell photoionization of tungsten. Phys. Rev. A 93 (2016) 033409.
7. G. Singh et al. Alignment of $L_3$ subshell vacancy states created without Coster–Kronig decay through selective photoionization in $_{82}$Pb, $_{90}$Th and $_{92}$U and effect of external magnetic field. Eur. Phys. J. D 71 (2017) 248.
8. A. Sharma. Inner shell alignment of atoms in photon impact ionization. J. Electron Spectrosc. Relat. Phenom. 225 (2018) 1.
9. D.H. Zhang, C.Z. Dong, Z.W. Wu. Angular distribution and polarization of characteristic x-ray lines following innershell photoionization of tungsten by linearly polarized light. J. Quant. Spectrosc. Radiat. Transf. 244 (2020) 106844.
10. V.K. Garg, R. Mittal, A. Sharma. Theoretical angular dependence of $L_3$ sub-shell X-rays following photoionization. J. Electron Spectrosc. Relat. Phenom. 248 (2021) 147054.
11. V.K. Garg, R. Mittal, A. Sharma. Non-relativistic dipole approximation based angular dependence of $L_3$ sub-shell X-rays following photoionization. AIP Conf. Proc. 2357 (2022) 070009.
12. Z.W. Wu, W. Liu, S. Fritzsche. Angular and polarization properties of characteristic x-ray radiation following inner-shell $2p_{3/2}$ photoionization of high-$Z$ atoms. Phys. Rev. A 108 (2023) 053115.
13. T. Luo et al. Linear polarization of x rays emitted in radiative recombination into the $K$ and $L$ shells of Kr, Xe, Bi, and U ions. Phys. Rev. A 109 (2024) 012822.
14. V.K. Garg et al. Linear polarization of $L_3$ sub-shell X-ray lines for some high-Z elements. Indian J. Phys. 98 (2024) 3445.
15. S. Käbisch et al. Polarity driven morphology of zinc oxide nanostructure. Appl. Phys. Lett. 103 (2013) 103106.
16. M. Al-Qadi et al. L-shell X-ray fluorescence relative intensities for elements with $64 \leq Z \leq 83$ at 21 keV and 25 keV by synchrotron radiation. J. Quant. Spectrosc. Radiat. Transf. 338 (2025) 109398.
17. L. Ábrók et al. Non-dipole anisotropy parameters in the photoionization of Kr in the region of deep inner shell excitations. J. Electron Spectrosc. Relat. Phenom. 258 (2022) 147209.
18. K. Verma et al. Experimental determination of L-subshells x-ray yields and production cross sections of thick lead (Z=82) element by impact of 15–30 keV electrons. J. Electron Spectrosc. Relat. Phenom. 280 (2025) 147541.
19. K.S. Kahlon et al. Linear polarization of $L\alpha_1$ and $L\alpha_2$ x-ray lines of gold. Phys. Rev. A 48 (1993) 1701.

**В. К. Гарг[1], М. Гупта[1], М. К. Тіварі[2], А. Шарма[1,*]**

[1] *Школа інженерії та технологій Читкара, Університет Читкара, Хімачал-Прадеш, Індія*
[2] *Центр передових технологій імені Раджі Раманни, Індор, Індія*

*Відповідальний автор: ajay.sharma@chitkarauniversity.edu.in

## ТЕОРЕТИЧНИЙ АНАЛІЗ АНІЗОТРОПІЇ ТА ПОЛЯРИЗАЦІЇ *L*-РЕНТГЕНІВСЬКОГО ВИПРОМІНЮВАННЯ ЕЛЕМЕНТІВ З ВИСОКИМ АТОМНИМ НОМЕРОМ *Z*

Представлено комплексне теоретичне дослідження кутової анізотропії та лінійної поляризації характеристичного рентгенівського випромінювання $L$-оболонки атомів з високим $Z$ (тантал, вольфрам, реній, іридій, золото та талій), що виникає внаслідок фотоіонізації неполяризованими фотонами. Розрахунки виконано в межах недипольного наближення з використанням трьох альтернативних моделей атомного потенціалу: (i) точкове кулонівське поле, (ii) екрановане кулонівське поле та (iii) аналітичний підхід на основі теорії збурень. Для дослідження виключно прямої флуоресценції $L$-оболонки енергію падаючих фотонів обмежено діапазоном від порога поглинання на $L$-підоболонках до межі $K$-оболонки; це дало змогу усунути внески від іонізації $K$-оболонки, переходів Костера–Кроніга та процесів міжоболонкового перенесення вакансій. Розраховано ступінь лінійної поляризації для спектральних ліній $L_\ell$, $L_{\alpha1}$ та $L_{\alpha2}$ в діапазоні енергій до 60 кеВ з метою визначення залежності цих параметрів від енергії збудження. Результати свідчать, що вирівнювання вакансій досягає максимуму поблизу порога іонізації, де відбуваються суттєві зміни амплітуд іонізації підоболонок та парціальних хвильових компонент фотоелектронів. Зі збільшенням енергії фотонів ступінь вирівнювання поступово зменшується, що призводить до зниження анізотропії та поляризації, а згодом наближається до граничного значення, яке повільно змінюється в області високих енергій. Перехід $L_\ell$ демонструє вищу анізотропію порівняно з лініями $L_\alpha$, тоді як значення поляризації для ліній $L_\ell$, $L_{\alpha1}$ та $L_{\alpha2}$ залишаються специфічними для кожного переходу через відмінності у зв'язку кутових моментів та матричних елементах радіаційних переходів. Для всіх досліджуваних елементів спостерігається закономірна залежність від атомного номера, причому важчі атоми демонструють відносно більші зміни характеру поляризації. Ця тенденція, ймовірно, відображає сукупний вплив релятивістських ефектів, спін-орбітальної взаємодії та ефектів електронної кореляції, характерних для важких атомних систем. Хоча всі три теоретичні підходи передбачають схожі загальні тенденції залежності від енергії, отримано помітні кількісні розбіжності у значеннях поляризації, що демонструє чутливість результатів до обраної моделі потенціалу та методу врахування вирівнювання вакансій. Проведене порівняння з раніше опублікованими результатами досліджень Kämpfer et al., а також Özdemir et al. підтверджує узгодженість виконаних розрахунків і забезпечує глибше теоретичне розуміння сукупного впливу вирівнювання вакансій, змішування мультиполів та релятивістської динаміки на рентгенівське випромінювання $L$-оболонки.

*Ключові слова:* рентгенівське випромінювання $L$-оболонки, поляризація, анізотропія, фотоіонізація, атоми з високим $Z$.

Надійшла / Received 05.05.2026